Porphyrin Derivatives for Telomere Binding and Telomerase Inhibition

Isabelle M. Dixon,[a] Frédéric Lopez,[b] Jean-Pierre Estève,[c] Agueda M. Tejera,[d] María A. Blasco,[d] Geneviève Pratviel,*[a] and Bernard Meunier*[a]

The capacity of G-quadruplex ligands to stabilize four-stranded DNA makes them able to inhibit telomerase, which is involved in tumour cell proliferation. A series of cationic metalloporphyrin derivatives was prepared by making variations on a meso*-tetrakis(4-*N*-methyl-pyridiniumyl)porphyrin skeleton (TMPyP). The DNA binding properties of nickel(II) and manganese(III) porphyrins were studied by surface plasmon resonance, and the capacity of the nickel porphyrins to inhibit telomerase was tested in a TRAP assay. The nature of the metal influences the kinetics (the process is faster for Ni than for Mn) and the mode of interaction (stacking or external binding). The chemical alterations did not lead to increased telomerase inhibition. The best selectivity for G-quadruplex DNA was observed for Mn-TMPyP, which has a tenfold preference for quadruplex over duplex.*

Introduction

Four strands of DNA can associate into a unique tetrahelical structure called a G-quadruplex that consists of stacked tetrads, which are each planar and stabilized by Hoogsteen-bonded guanines. The formation of G-quadruplexes in vitro is stabilized by the presence of monovalent cations (K^+, Na^+) positioned in the centre of the structure and coordinated to the carbonyl oxygens (Scheme 1). Guanine-rich sequences able

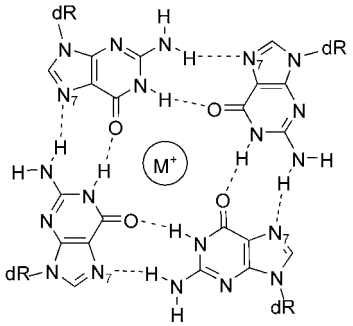

Scheme 1. *Structure of a G-tetrad showing the Hoogsteen base pairing.*

to form G-quadruplexes are found in many chromosomal locations, such as the end of the chromosomes, in the telomeric region,[1,2] in gene promoters, especially the proto-oncogene c-*myc*,[3,4] in the immunoglobulin switch region,[5] and at the DNA flap of HIV-1.[6,7] The formation of G-quadruplex structures under physiological conditions in vivo, as well as the selective interaction or binding of several specific proteins with quadruplex DNA, suggest that tetrahelical DNA may be formed in vivo.[8–13]

Because of their unique structural features and possible cellular function, G-quadruplexes constitute an attractive target for drug design. In particular, the design of small molecules able to target the telomeric G-quadruplex structure seems a promising strategy for new antitumour drugs.[14,15] Telomeres at the end of eukaryotic chromosomes are maintained by telomerase, a ribonucleoprotein enzyme. In most human somatic cells, telomerase is repressed and telomeres shorten progressively with each cell division. In contrast, most human tumours express telomerase; this results in stabilized telomere length. Thus, G-quadruplex-interacting drugs have the potential to inhibit telomerase-mediated elongation of telomeres by stabilizing G-quadruplexes and could therefore stop the proliferation of tumour cells.

Human telomeric DNA consists of double-stranded d(TTAGGG/CCCTAA) repeats and a single-stranded 3′ overhang. This single-stranded sequence adopts an intramolecular G-quadruplex structure in vitro. The NMR-based structure of an intramolecular quadruplex with anti-parallel strands and three d(TTA) loops stacked onto the end of the G-quartet was report-

[a] *Dr. I. M. Dixon, Dr. G. Pratviel, Dr. B. Meunier*
Laboratoire de Chimie de Coordination, CNRS UPR 8241
205 route de Narbonne, 31077 Toulouse Cedex 4 (France)
Fax (+33) 561-553-003
E-mail: pratviel@lcc-toulouse.fr
bmeunier@lcc-toulouse.fr

[b] *Dr. F. Lopez*
INSERM IFR 31, Institut Louis Bugnard
Hôpital Rangueil, TSA 50032
31059 Toulouse Cedex 9 (France)

[c] *Dr. J.-P. Estève*
INSERM U 531, Institut Louis Bugnard
Hôpital Rangueil, TSA 50032
31059 Toulouse Cedex 9 (France)

[d] *Dr. A. M. Tejera, Dr. M. A. Blasco*
Spanish National Cancer Center
Melchor Fernández Almagro 3, 28029 Madrid (Spain)

Supporting information for this article is available on the WWW under http://www.chembiochem.org or from the author: full NMR assignments, sensorgram for the interaction of ***4****·NiNi with quadruplex DNA, sensorgrams for the interaction of all molecules with GC and AT duplexes and corresponding Scatchard plots, pictures of the TRAP assay gels for* ***3****·Ni and* ***4****·NiNi.*

 DOI: 10.1002/cbic.200400113

ed with the 22-mer oligonucleotide model d(AGGG(TTA GGG)$_3$).[16] The same human telomeric sequence crystallized in a different way with all the strands parallel and the resulting diagonal loops oriented away from G-quartets.[17] It was recently shown that the two structures may exist in solution.[18] However, this sequence still represents a convenient simplified model for the in vitro screening of drugs able to target telomeric DNA. Several G-quadruplex-interactive compounds have been identified. Most quadruplex ligands are polyaromatic molecules bearing one or more positive charge(s) and are able to interact by stacking with G-tetrads.[19–28] In addition, some compounds that interact with the grooves of G-quadruplexes have also been reported.[29,30]

Among the compounds able to have stacking interactions with G-quadruplex DNA is the nonmetallated cationic porphyrin, *meso*-tetrakis(4-*N*-methylpyridiniumyl)porphyrin, H_2-TMPyP (**1**·H_2) (Scheme 2).[19] After photochemical activation, this porphyrin derivative was shown to react with the guanine bases of the last tetrad of the G-quadruplex structure; this implies that it stacks externally to the G-tetrads located at the end of the G-quadruplex. **1**·H_2 inhibited telomerase in TRAP assays in vitro with an IC_{50} of 6.5 μM.[19] This compound was taken as a basic structure for the present work. A series of metalloporphyrins was prepared with structural modifications based on a common tris(*N*-methylpyridiniumyl) porphyrin to try to improve the G-quadruplex-targetting properties of the starting **1**·H_2.

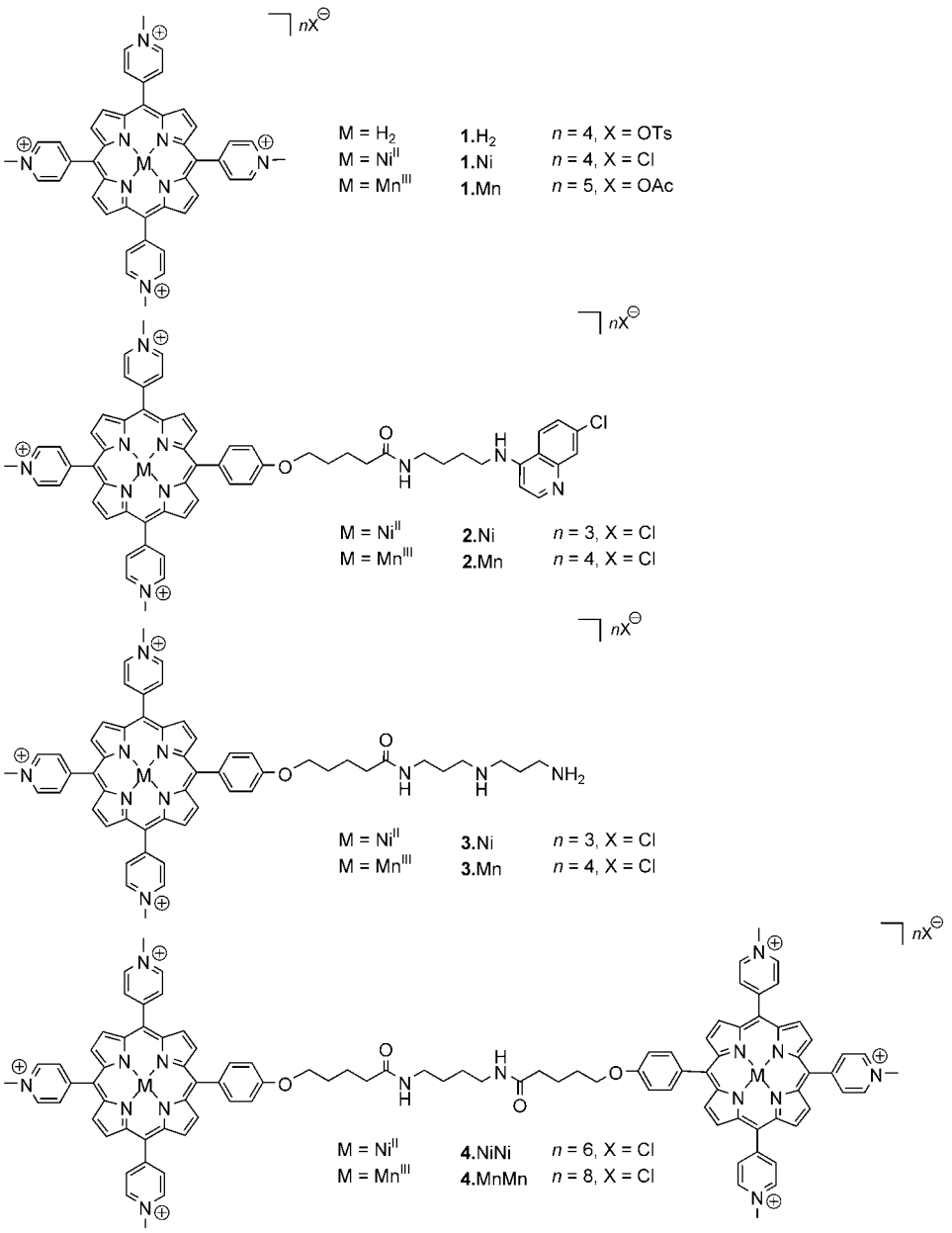

Scheme 2. *Chemical formulae of the molecules studied (Mn stands for $Mn^{III}(H_2O)_2$).*

Two types of metalloporphyrins were prepared by metallation with nickel or manganese. Depending on the nature of the metal inside the porphyrin macrocycle, the mechanism of action of these molecules towards telomeric sequences should be different. Nickel porphyrins are inert with respect to redox processes under physiological conditions and are not photoactivable. The Ni–porphyrin derivatives are thus going to interact with the telomeres in a passive way compared to the Mn–porphyrin derivatives, which should be able to interact with and degrade the telomeres by oxidative processes within cells. Furthermore, the nickel porphyrins are expected to interact by stacking, whereas stacking interactions are impossible for manganese porphyrins due to the presence of water as axial ligands on the manganese.[31]

The binding of these porphyrin derivatives to duplex and intramolecular quadruplex DNA was studied by surface plasmon resonance, and their capacity to inhibit telomerase was measured by TRAP assays. The data show that, within this series of metalloporphyrin derivatives, the kinetics of binding to DNA (k_{on}, k_{off}) were highly dependent on the nature of the central metal. The compounds tested for telomerase inhibition had similar IC_{50} values; this is in agreement with their similar affinity for G-quadruplex DNA. The molecule that is most selective for G-quadruplexes appears to be the simple Mn-TMPyP (**1**·Mn), which is not able to interact by stacking interaction

with a G-tetrad due to the presence of axial ligands on the metal. **1**·Mn probably binds the G-quadruplex by interaction in the grooves, and this interaction leads to a binding affinity that is in the same range as one reached by stacking. Furthermore, this series of molecules allowed us to notice that the kinetics of drug interaction with G-quadruplex DNA seem to depend on the mode of binding, stacking versus external binding.

Results and Discussion

The starting point for this study lies in the interesting interactions that have been shown to take place between H_2-TMPyP (**1**·H_2) and quadruplex DNA.[19] From the location of the damage resulting from photochemical irradiation, it was deduced that the porphyrin interacts with this particular DNA structure by stacking on the last guanine tetrad. This propensity of porphyrins for stacking can be exploited to design new G-quadruplex-interacting compounds with potential applications in cancer therapy. Chemical modifications have been made to the porphyrin skeleton to try to improve the quadruplex affinity and selectivity over double-stranded DNA.

Synthesis

All the molecules studied here share a tris(*N*-methylpyridiniumyl)porphyrin core. The starting motif **1** is *meso*-tetrakis(4-*N*-methylpyridiniumyl)porphyrin, either as free base (**1**·H_2) or metallated with nickel(II) or manganese(III). **1**·H_2 was metallated by nickel(II) to give **1**·Ni, in which nickel does not bear axial ligands (Scheme 2). This porphyrin should interact with G-quadruplexes in a way similar to the nonmetallated derivative **1**·H_2, that is, by stacking with the last G-tetrad. The manganese(III) derivative of **1**·H_2, **1**·Mn (Scheme 2), carries two axial ligands on the manganese ion. This should preclude a strong stacking interaction with the G-tetrads. However, this compound is able to interact with quadruplex DNA since it is very efficient in the degradation of quadruplex DNA of the human telomeric sequence.[32] The damage was shown to take place at the external tetrad of the quadruplex structure, at the junction between the quadruplex and the duplex region of the tested DNA substrate.

The other porphyrins **2**, **3** and **4** have a hybrid structure composed of two chemical moieties that may contribute in their own specific way to the binding process. In the case of **2**,[33] an aminoquinoline motif was chosen for its capacity to stack with aromatics in general and nucleic bases in particular. Molecule **3** bears a polyamine side chain, which gets protonated in water and can interact with DNA grooves by ionic interactions. The bisporphyrinic skeleton of molecule **4** was selected, in combination with a linker of appropriate length, for the possible formation of a sandwich-type interaction complex with quadruplex DNA.

The synthesis of **3** and **4** (Scheme 3) starts with the two-step preparation of porphyrin **5** [34,35] and its condensation with either bis(3-aminopropyl)amine or 1,4-diaminobutane. After quaternization of the pyridine nitrogens with methyl iodide, the porphyrin is metallated with nickel or manganese acetate, and chlorides are introduced as counter ions by treatment with an anion exchange resin.

Surface plasmon resonance (SPR)

The interaction of the molecules with DNA was studied by SPR. The 5′-biotin-labelled DNA was immobilized on a sensor chip through a biotin–streptavidin noncovalent coupling. Three DNA targets were simultaneously examined under salt conditions, which are suitable for quadruplex DNA (HBS-EP buffer from BIAcore supplemented with 200 mM KCl).[36] The binding of the molecules to a 22-mer GC-rich hairpin duplex (5′-TT$(CG)_4$TTTT$(CG)_4$) and a 20-mer AT-rich hairpin duplex (5′-CGAATTCGTCTCCGAATTCG) was compared to the binding to a preformed intramolecular 22-mer quadruplex containing three repeats of the human telomeric sequence (5′-AGGG$(TTAGGG)_3$). Sensorgrams (resonance units, RU, versus time) for the concentration-dependent binding of the porphyrin derivatives on the quadruplex DNA are shown in Figure 1, with the corresponding Scatchard plots on the right.

Binding constants are highly dependent on ionic strength, especially in the cases in which ionic interactions are important contributors to the binding. This, in addition to the fact that SPR is a heterogeneous technique (the DNA is fixed on a surface), means that no direct comparison can be made between binding constants determined in solution under different conditions by other techniques [37–39] and binding constants determined by SPR. However results obtained by SPR under similar experimental conditions can be compared. In the literature there are few examples of quadruplex binding constants determined by SPR. Ditercalinium associates with quadruplex DNA with a high affinity constant ($K_a = 3\times10^7\ M^{-1}$), but its selectivity is only modest, a factor of 3.[36] A bisquinacridine macrocycle has an affinity constant of $1.2\times10^7\ M^{-1}$ and its selectivity is one order of magnitude in favour of the quadruplex.[27] A peptide–hemicyanine conjugate (Phe-Arg-His-Arg-hemicyanine) binds quadruplex DNA with a relatively low affinity constant ($K_a = 6.8\times10^4\ M^{-1}$), but it has a 40-fold selectivity for quadruplex.[30] The best combination of affinity and selectivity so far reported

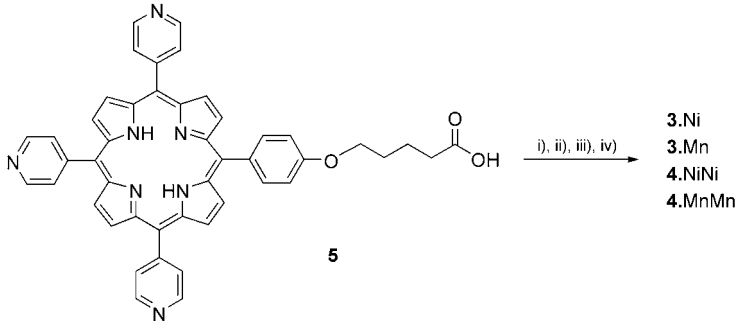

Scheme 3. *Synthetic pathway for the synthesis of metalloporphyrins **3** and **4** from porphyrin **5**. i) bis(3-aminopropyl)amine or 1,4-diaminobutane, BOP, NMM. ii) CH_3I. iii) $Ni(OAc)_2$ or $Mn(OAc)_2$. iv) DOWEX 1×8–200, chloride form.*

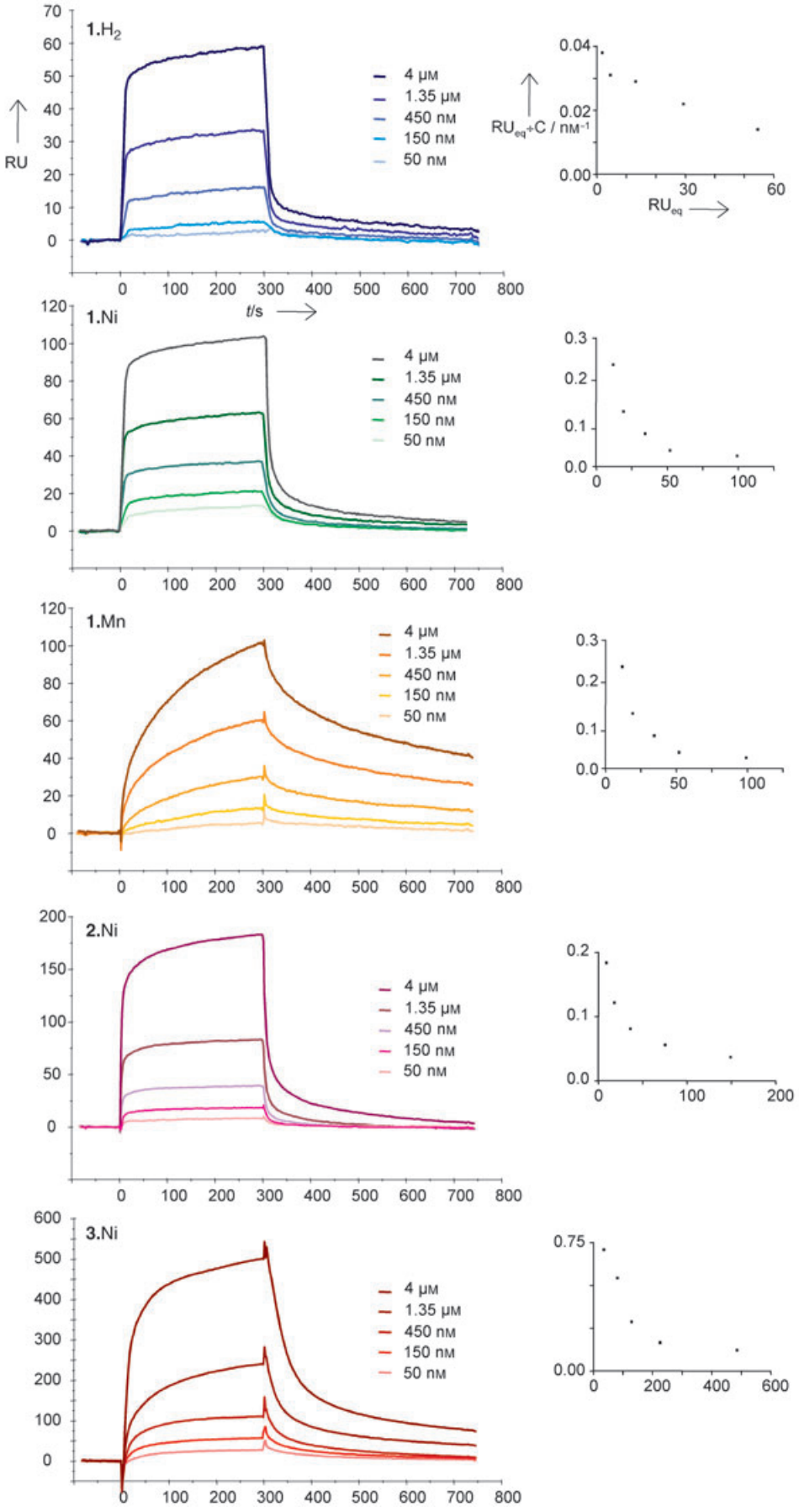

is for a 3,6,9-trisubstituted acridine designed by molecular modelling, which has an affinity constant of $1.6\times10^{7}\,M^{-1}$ and a 40-fold preference for quadruplex over duplex.[21]

The sensorgrams (Figure 1) show that the amount of bound molecule is highly variable from one molecule to another (see response at $t = 300$ s). In four cases (**1**·H_2, **1**·Ni, **1**·Mn and **2**·Ni), the response at 300 s is around 100 RU, but this value rises to about 500 RU for **3**·Ni and it even goes up to about 1500 RU for **4**·NiNi (see Supporting Information). This shows that the amount of bound **4**·NiNi is very high, which could be explained by the formation of aggregates. It has to be noted that this tendency of **4**·NiNi for aggregation was not observed in water at micromolar concentrations (UV-visible spectra, not shown), while the concentrations for SPR analysis ranged from 50 nM to 4 μM, therefore this phenomenon seems to be facilitated by DNA. The calculation of association and dissociation kinetics would be biased by the aggregation of **4**·NiNi, and so would be the calculation of the affinity constant. The behaviour of **4**·NiNi was therefore considered to be uninterpretable, and for this reason the sensorgram and the corresponding constants are not shown.

The sensorgrams show two distinct trends. On the one hand,

Figure 1. *Sensorgrams for molecules* **1**·H_2, **1**·Ni, **1**·Mn, **2**·Ni *and* **3**·Ni *on quadruplex DNA, with the corresponding Scatchard plots on the right. All tested molecules were injected on flow cells at a flow rate of 20 μL min^{-1} and exposed to the surface for 300 s (association phase) followed by a 300 s flow running during which dissociation occurred. Molecules were injected at different concentrations ranging from 50 nM to 4 μM in HBS-EP buffer supplemented with 200 mM KCl. Results are expressed in resonance units (RU) as a function of time in seconds.*

in the case of **1**·Mn, the DNA binding sites are not saturated by the end of the porphyrin injection, and this behaviour corresponds to slow kinetics of interaction. On the other hand, for all the other molecules, the response reaches a plateau within the first 300 s of the experiment; this means that the binding is fast.

Table 1 summarizes the kinetic constants for the association and dissociation of the molecules with GC duplex, AT duplex and quadruplex DNA. From these kinetic constants the corresponding affinity constants (K_a) were calculated. Scatchard graphs were plotted for each molecule and each DNA target (see Supporting Information) in order to determine the relevance of a one-site or a nonequivalent two-site model. The relevance of the model was subsequently validated by the goodness of fit of the BIAeval model applied to each sensorgram. In cases in which the experimental data were fitted with a nonequivalent two-site model, the constants discussed correspond to the site of higher affinity. Under the experimental conditions used for SPR analysis (200 mM KCl), one molecule (**1**·Ni) has higher affinity for duplex ($10^7\,M^{-1}$) than for quadruplex ($10^6\,M^{-1}$), three molecules (**1**·H_2, **2**·Ni, **3**·Ni) have similar affinity for duplex and quadruplex ($10^6\,M^{-1}$), and one molecule (**1**·Mn) has higher affinity for quadruplex ($10^7\,M^{-1}$) than for duplex ($10^6\,M^{-1}$).

Table 1. *Kinetic constants for the association (k_{on} [$M^{-1}s^{-1}$]) and dissociation (k_{off} [s^{-1}]) of the given molecules with GC duplex, AT duplex and quadruplex DNA, and corresponding affinity constants (K_a [M^{-1}]). When fitted with a nonequivalent two-site model, the second set of values corresponds to the site of lower affinity.*

		1·H_2	**1**·Ni	**1**·Mn	**2**·Ni	**3**·Ni
GC duplex	k_{on}	339×10^3	368×10^3	0.95×10^3	265×10^3	65.8×10^3
		145×10^3	–	–	2.13×10^3	1.36×10^3
	k_{off}	201×10^{-3}	46×10^{-3}	2.72×10^{-3}	262×10^{-3}	33.3×10^{-3}
		433×10^{-3}	–	–	3.39×10^{-3}	2.56×10^{-3}
	K_a	1.69×10^6	8×10^6	0.35×10^6	1.01×10^6	1.98×10^6
		0.33×10^6	–	–	0.63×10^6	0.53×10^6
AT duplex	k_{on}	44.6×10^3	546×10^3	1.67×10^3	233×10^3	2.03×10^3
		37.2×10^3	1.41×10^3	–	10.2×10^3	21.3×10^3
	k_{off}	24.5×10^{-3}	35.1×10^{-3}	1.74×10^{-3}	73.4×10^{-3}	1.27×10^{-3}
		23.8×10^{-3}	3.29×10^{-3}	–	15.4×10^{-3}	26.0×10^{-3}
	K_a	1.82×10^6	15.6×10^6	0.96×10^6	3.17×10^6	1.60×10^6
		1.56×10^6	0.43×10^6	–	0.66×10^6	0.82×10^6
Quadruplex	k_{on}	4.75×10^3	74.4×10^3	27.2×10^3	82.9×10^3	0.011×10^3
		–	3.05×10^3	0.26×10^3	0.59×10^3	7.99×10^3
	k_{off}	6.60×10^{-3}	44.6×10^{-3}	3.35×10^{-3}	161×10^{-3}	0.003×10^{-3}
		–	3.35×10^{-3}	1.65×10^{-3}	8.86×10^{-3}	16×10^{-3}
	K_a	0.72×10^6	1.67×10^6	8.12×10^6	0.51×10^6	3.66×10^6
		–	0.91×10^6	0.16×10^6	0.07×10^6	0.50×10^6

In summary, one molecule stands out of this series, namely **1**·Mn. It is interesting both in terms of affinity for quadruplex DNA ($K_a = 8\times10^6\,M^{-1}$) and in terms of selectivity for quadruplex over duplex, by one order of magnitude. To test the hypothesis that manganese(III), possibly because of its axial ligands, was responsible for such behaviour, a second series of molecules was synthesized and analyzed by SPR (Figure 2). **1**·Mn was measured once more and taken as a reference for this second series of measurements.

The sensorgram obtained for the interaction of **1**·Mn with the DNA quadruplex has the same shape as in the first series of measurements (Figure 2). Three molecules of the series (**1**·Mn, **3**·Mn, **4**·MnMn) show signals which are far from saturation. Only in one case does the signal almost reach a plateau within the time frame of the analysis (300 s), that is **2**·Mn. Unlike in the case of the nickel(II) analogues, the highest RU values observed (350 for **4**·MnMn) are consistent with the absence of aggregation, as expected for such metalloporphyrins bearing axial ligands.

The association and dissociation kinetic constants and the affinity constants of the manganese-based molecules with GC duplex, AT duplex and quadruplex DNA are reported in Table 2. The affinity constants of all the manganese porphyrins for duplex DNA are in the range 10^5–$10^7\,M^{-1}$. This is slightly higher than their nickel(II) counterparts, and the values can be explained by the additional positive charge brought by the trivalent metal ion. The major difference stands in the kinetics of interaction, which are slower in the case of Mn^{III}. One exception is found for **2**·Mn, which is particular within this second series because it contains an aromatic quinoline moiety. It is noteworthy that **2**·Mn shows an 80-fold preference for GC duplex over AT duplex. On the other hand, **3**·Mn has the highest affinity of all porphyrins tested (nearly $10^8\,M^{-1}$ for quadruplex DNA), but this is not accompanied by selectivity.

Comparison of the two sets of data leads us to propose different interaction modes for the molecules depending on their slow or fast kinetics of interaction. All the fast-binding molecules (**1**·H_2, **1**·Ni, **2**·Ni, **3**·Ni, **2**·Mn) have in common an aromatic moiety that is capable of interacting with DNA by stacking. Both **2**·Ni and **2**·Mn contain a quinoline substituent, which should be able to stack with a guanine tetrad and may govern the interaction of the conjugate with DNA. On the other hand, the slow-binding molecules (**1**·Mn, **3**·Mn, **4**·MnMn) all contain a manganese porphyrin, and these slower kinetics could be explained either by the perturbation of the coordination sphere of the metal ion upon interaction with DNA, or, more likely, by a binding mode that is different from stacking (external binding).

TRAP assay

The cell-free enzyme-based telomeric repeat amplification protocol (TRAP) assay was performed with **3**·Ni and **4**·NiNi to determine whether these new molecules could be telomerase in-

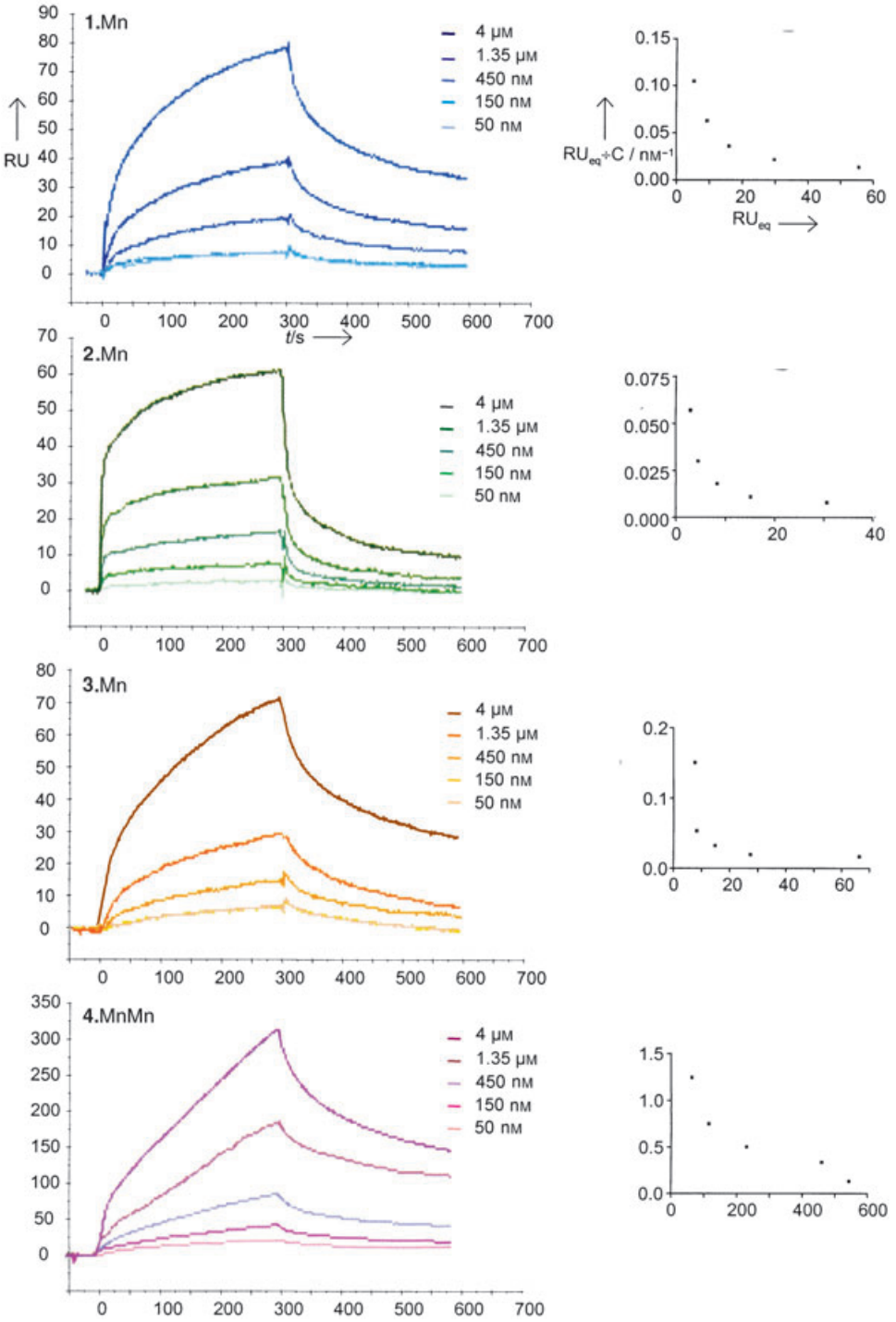

Figure 2. *Sensorgrams for molecules* ***1***·*Mn,* ***2***·*Mn,* ***3***·*Mn and* ***4***·*MnMn on quadruplex DNA, with the corresponding Scatchard plots on the right. All tested molecules were injected on flow cells at a flow rate of 20 μL min^{-1} and exposed to the surface for 300 s (association phase) followed by a 300 s flow running during which the dissociation occurred. Molecules were injected at different concentrations ranging from 50 nM to 4 μM in HBS-EP buffer supplemented with 200 mM KCl. Results are expressed in resonance units (RU) as a function of time in seconds.*

hibitors. The two compounds caused inhibition of telomerase-mediated elongation of the telomere primer at micromolar concentrations. The IC_{50} values are given in Table 3. The similar values obtained for telomerase inhibition are consistent with the similar affinity constants found by SPR. This seems again to indicate that the tris(*N*-methylpyridiniumyl)porphyrin moiety is predominantly responsible for the porphyrin–DNA interactions.

Conclusion

A series of nickel and manganese porphyrin derivatives has been prepared and the derivatives have been compared for their ability to target G-quadruplex DNA. Within this series, two different modes of interaction with an intramolecular G-quadruplex structure were proposed on the basis of surface plasmon resonance experimental data. Relatively fast kinetics were observed for all molecules containing a moiety that can interact by stacking with the last guanine tetrad of the quadruplex (free base or nickel porphyrin, quinoline). On the other hand, slow kinetics were observed for manganese porphyrins, for which stacking is not possible due to axial ligands on the manganese ion. Hindering stacking slows down the interaction and, hence, leads to better affinity and selectivity, as observed for the manganese porphyrin **1**·Mn. This raises the possibility that stacking may not be the best means of achieving high affinity and selectivity for G-quadruplex structures. Targetting G-quadruplex DNA in an external manner through groove interaction should allow for discrimination between the various G-quadruplex structures that may exist in vivo.

Experimental Section

Synthesis: The following compounds were commercially available: bis(3-aminopropyl)amine (Aldrich, dried over KOH), NaOH (Fluka, small beads), *N*-methylmorpholine (NMM, Fluka, dried over KOH), benzotriazol-1-yloxytris(dimethylamino)phosphonium hexafluorophosphate (BOP, Fluka), HCl (1 M) in diethyl ether (Aldrich), methyl iodide (Aldrich), potassium hexafluorophosphate (Fluka), nickel(II) acetate tetrahydrate (Aldrich), manganese(II) acetate tetrahydrate (Fluka), 2,4,6-collidine (Aldrich), DOWEX 1×8–200 resin (chloride form, Acros), 1,4-diami-

Table 2. *Kinetic constants for the association (k_{on} [$M^{-1}s^{-1}$]) and dissociation (k_{off} [s^{-1}]) of the given molecules with GC duplex, AT duplex and quadruplex DNA, and corresponding affinity constants (K_a [M^{-1}]). When fitted with a nonequivalent two-site model, the second set of values corresponds to the site of lower affinity.*

		1·Mn	**2**·Mn	**3**·Mn	**4**·MnMn[a]
GC duplex	k_{on}	0.42×10^{3}	3540×10^{3}	0.12×10^{3}	0.35×10^{3}
		–	0.86×10^{3}	0.79×10^{3}	–
	k_{off}	3.66×10^{-3}	153×10^{-3}	0.012×10^{-3}	2.52×10^{-3}
		–	15×10^{-3}	10.5×10^{-3}	–
	K_a	0.11×10^{6}	23.14×10^{6}	10.0×10^{6}	0.14×10^{6}
		–	0.06×10^{6}	0.07×10^{6}	–
AT duplex	k_{on}	0.81×10^{3}	3.23×10^{3}	0.18×10^{3}	5.27×10^{3}
		–	–	1.38×10^{3}	–
	k_{off}	3.05×10^{-3}	10.9×10^{-3}	0.004×10^{-3}	3.24×10^{-3}
		–	–	12.0×10^{-3}	–
	K_a	0.27×10^{6}	0.30×10^{6}	45.0×10^{6}	1.63×10^{6}
		–	–	0.11×10^{6}	–
Quadruplex	k_{on}	52.9×10^{3}	174×10^{3}	0.23×10^{3}	2.36×10^{3}
		1.19×10^{3}	1.05×10^{3}	1.10×10^{3}	–
	k_{off}	19.2×10^{-3}	103×10^{-3}	0.003×10^{-3}	2.07×10^{-3}
		1.56×10^{-3}	4.65×10^{-3}	7.22×10^{-3}	–
	K_a	2.76×10^{6}	1.69×10^{6}	76.7×10^{6}	1.14×10^{6}
		0.76×10^{6}	0.23×10^{6}	0.15×10^{6}	–

[a] Fitted with a one-site Langmuir model. Fitting was not improved by using a two-site model; this reflects the complexity of the interaction (as seen in the shape of the sensorgrams).

Table 3. *IC_{50} values [μM] for the inhibition of telomerase, measured in a TRAP assay.*

	1·H_2	**1**·Ni	**1**·Mn	**2**·Ni	**3**·Ni	**4**·NiNi
IC_{50}	6.5[a]	5[b]	25.9[b]	7.3[b]	12.8	9.9

[a] From ref. [19]. [b] From ref. [33].

nobutane (Janssen), *meso*-tetrakis(*N*-methylpyridiniumyl)porphyrin tetra-*p*-tosylate (Aldrich). Porphyrin **5**, **1**·Ni, and **1**·Mn were prepared according to literature procedures.[34,35] Molecules **2**·Ni and **2**·Mn had been obtained from previous studies.[33] Silica gel refers to Merck 63–200 μm silica (ref. 107734) and alumina refers to neutral Merck alumina (ref. 101077). TLC analysis was performed with Merck 60 F_{254} silica-coated aluminium plates. Aqueous ammonium hydroxide solution was 28% by weight. DMF was dried over 4 Å molecular sieves. ^{1}H NMR spectra were recorded on a Bruker Avance 300 spectrometer with the residual solvent peak as internal calibration. Mass spectra were recorded either on a Perkin–Elmer SCIEX API 365 (electrospray) or on a Nermag R1010 apparatus (chemical ionization). UV-visible spectra were recorded on a Hewlett Packard 8452A spectrophotometer.

Synthesis of 6: Freshly dried **5** (190 mg, 0.26 mmol) was dissolved in bis(3-aminopropyl)amine (>500 equiv, 20 mL) under argon. NMM (50 eq, 1.5 mL) and BOP (2 eq, 245 mg) were added, and the reaction mixture was stirred at room temperature overnight. One more equivalent of BOP was added, and the mixture was stirred for a further 4 h at room temperature. The crude mixture was diluted with water (150 mL) and extracted with CH_2Cl_2 (3×50 mL) and $CHCl_3$ (50 mL). The dark red organic layer was evaporated to dryness. The product was purified by dissolution in $CHCl_3$ (20 mL) followed by precipitation at 4 °C with hexane (80 mL) overnight. Yield 46% (102 mg); purple solid; ^{1}H NMR (300 MHz, $CDCl_3$) $\delta=9.07$ (d, $^3J=6.0$ Hz, 6H), 9.00 (d, $^3J=4.8$ Hz, 2H), 8.87 (s, 4H), 8.83 (d, $^3J=4.8$ Hz, 2H), 8.18 (d, $^3J=5.9$ Hz, 6H), 8.12 (d, $^3J=8.7$ Hz, 2H), 7.31 (d, $^3J=8.9$ Hz, 2H), 4.31 (t, $^3J=7.5$ Hz, 2H), 3.44 (m, 2H), 2.83 (m, 2H), 2.76 (t, $^3J=7.5$ Hz, 2H), 2.48 (m, 2H), 2.05 (m, 4H), 1.62 (m, 2H), 1.47 (m, 2H), 0.89 (t, $^3J=7.4$ Hz, 2H), −2.86 ppm (br s, 2H); CI-MS: 848 ($[M+H]^+$), 790 ($[M-(CH_2)_3NH_2+2H]^+$), 733 ($[M-(CH_2)_3NH-(CH_2)_3NH_2+2H]^+$), 634 ($[M-(CH_2)_4CONH(CH_2)_3NH(CH_2)_3NH_2+2H]^+$).

Synthesis of 7: Compound **6** (19 mg, 23 μmol) was dissolved in $CHCl_3$ (5 mL). 2 equivalents of HCl (1 M in Et_2O, 52 μL) were added to protonate the alkylamine functions; this caused partial precipitation of the porphyrin, which was solubilized by adding the minimum amount of MeOH (3 mL). Excess CH_3I (100 eq, 170 μL) was added, the flask was stoppered with a septum, and the reaction mixture was stirred at room temperature and in the dark over the weekend. The mixture was evaporated and taken in the minimum of MeCN/MeOH (1:1), the charged compounds were precipitated as hexafluorophosphate salts by adding saturated aqueous KPF_6 and evaporating the organic solvents. The precipitate was filtered on a fritted glass (porosity 4), washed thoroughly with water to eliminate inorganic salts and washed with CH_2Cl_2 and $CHCl_3$. The chlorinated filtrates were colourless; this shows that all starting material has disappeared. The precipitate was taken in MeOH and dried. Yield 100% (30 mg); purple-brown solid; ^{1}H NMR (300 MHz, CD_3CN), $\delta=9.02$ (m, 14H), 8.84 (m, 6H), 8.23 (m, 2H), 7.41 (m, 2H), 4.70 (s, 9H), 4.34 (m, 2H), 3.40 (m, 2H), 3,17 (m, 2H), 3.10 (m, 2H), 3.03 (m, 2H), 2.49 (m, 2H), 2.11 (m, 4H), 1.44 (m, 2H), −2.90 ppm (br s, 2H). NB: whatever the NMR solvent used (CD_3CN, CD_3OD, [D_6]acetone, [D_6]DMSO), some methylene peaks are superimposed with solvent and/or water peaks, hence in these four cases there are always less than ten clear methylene signals. ES$^+$-MS, *m/z*: 1181.6 ($[M-PF_6]^+$), 1167.5 ($[M-PF_6-CH_3+H]^+$), 1110.5 ($[M-PF_6-CH_3+H-(CH_2)_3NH_2]^+$), 1021.5 ($[M-2PF_6-CH_3]^+$), 1007.5 ($[M-2PF_6-2CH_3+H]^+$), 804.4 ($[M-3PF_6-2CH_3+H-(CH_2)_3NH_2]^+$), 747.4 ($[M-3PF_6-2CH_3+H-(CH_2)_3NH(CH_2)_3NH_2]^+$), 647.3 ($[M-3PF_6-2CH_3+H-(CH_2)_4CONH(CH_2)_3NH(CH_2)_3NH_2]^+$), 518.5 ($[M-2PF_6]^{2+}$), 511.3 ($[M-2PF_6-CH_3+H]^{2+}$), 438.4($[M-3PF_6-CH_3]^{2+}$), 409.9 ($[(M-3PF_6-CH_3-(CH_2)_3NH_2]^{2+}$), 331.5 ($[M-3PF_6-CH_3+H-(CH_2)_4-CONH(CH_2)_3NH(CH_2)_3NH_2]^{2+}$).

Synthesis of 3·Ni: Compound **7** (14 mg, 10 μmol) and nickel(II) acetate tetrahydrate (3 equiv, 7.5 mg) were heated in DMF (1 mL) and 2,4,6-collidine (0.5 mL) at 110 °C in the dark for 3 h. The product was precipitated as a hexafluorophosphate salt by adding saturated aqueous KPF_6, filtered on a fritted glass (porosity 4), washed with water, taken in acetone and dried. Yield 90% (12.5 mg); red-orange solid.

Anion exchange was performed on DOWEX 1×8–200 resin (chloride form) by stirring a suspension of the porphyrin in water (15 mL) at 50 °C for 48 h. The resin was filtered on a fritted glass (porosity 3) and washed with MeOH, MeCN and H_2O. The solvents were evaporated, the product was taken in MeOH and dried. Yield 100% (11 mg); red-orange solid. ES$^+$-MS: *m/z*: 917.6 ($[M-3Cl-2CH_3-H]^+$), 903.6 ($[M-3Cl-3CH_3]^+$), 458.8 ($[M-3Cl-2CH_3-H]^{2+}$), 451.8 ($[M-3Cl-3CH_3]^{2+}$). UV/Vis (H_2O) λ_{max} (ε) = 418 (78500), 532 nm (7400 $mol^{-1}\,L\,cm^{-1}$).

Synthesis of 3·Mn: Compound **7** (14 mg, 10 μmol) and manganese(II) acetate tetrahydrate (8 equiv, 20 mg) were heated in DMF (1 mL) and 2,4,6-collidine (0.5 mL) at 110 °C in the dark for $2^1/_2$ h. A second batch of $Mn(OAc)_2\cdot4H_2O$ (8 equiv, 20 mg) was added as an aqueous solution (0.5 mL), and heating was maintained for an additional $3^1/_2$ h. The product was precipitated as a hexafluorophosphate salt by adding saturated aqueous KPF_6, filtered on a fritted

glass (porosity 4), washed with water, taken in acetone and dried. Yield 78% (12 mg); green-brown solid.

Anion exchange was performed on DOWEX 1×8–200 resin (chloride form) by stirring the porphyrin in water (25 mL) at 50°C for 48 h (final water volume 10 mL). The resin was filtered on a fritted glass (porosity 3) and washed with MeOH, MeCN and water. The solvents were evaporated, the product was taken in MeOH and precipitated with diethyl ether. The precipitate was filtered, washed with Et_2O, taken in MeOH and dried. Yield 100% (10 mg); green-brown solid; ES^+-MS: *m/z*: 815.3 ($[M-4Cl-(CH_2)_3NH(CH_2)_3NH_2+H-CH_3]^+$), 800.4 ($[M-4Cl-(CH_2)_3NH(CH_2)_3NH_2+H-2CH_3]^+$), 785.3 ($[M-4Cl-(CH_2)_3NH(CH_2)_3NH_2+H-3CH_3]^+$), 407.7 ($[M-4Cl-(CH_2)_3NH(CH_2)_3NH_2+H-CH_3]^{2+}$), 400.3 ($[M-4Cl-(CH_2)_3NH(CH_2)_3NH_2+H-2CH_3]^{2+}$), 391.7 ($[M-4Cl-(CH_2)_3NH(CH_2)_3NH_2+H-3CH_3]^{2+}$); UV/Vis ($H_2O$) λ_{max} (ε) = 466 nm (40000 $mol^{-1}Lcm^{-1}$).

Synthesis of 8: Under anhydrous conditions, freshly dried **5** (90 mg, 0.123 mmol) was placed under argon and dissolved in dry DMF (10 mL). BOP (2 equiv, 109 mg) was added as a solid, followed by NMM (20 equiv, 0.27 mL). The reaction mixture was stirred at room temperature for 30 min to form the activated ester. 1,4-diaminobutane (0.75 equiv, 10 μL) was added, and the solution was stirred under argon at room temperature overnight. The porphyrinic products were precipitated by the addition of diethyl ether (80 mL), filtered and washed with Et_2O. The crude mixture contained only two major porphyrin bands and a trace of starting material, as shown by TLC (SiO_2, CH_2Cl_2/EtOH/aq. NH_4OH 90:10:0.5). Purification was achieved by silica gel column chromatography (height 30 cm, i.d. 2.8 cm). The desired bisporphyrin was first eluted with CH_2Cl_2/10% EtOH/1% NH_4OH (65 mg, 70%), and the 1:1 condensation product was eluted with CH_2Cl_2/15% MeOH/1% NH_4OH (30 mg, 30%). Purple solids; ^1H NMR (300 MHz, $CDCl_3$), δ = 9.05 (m, 4H), 9.02 (m, 8H), 8.95 (d, ^3J = 5 Hz, 4H), 8.84 (s, 8H), 8.79 (d, ^3J = 5 Hz, 4H), 8.15 (m, 4H), 8.13 (m, 8H), 8.09 (d, ^3J = 8.7 Hz, 4H), 7.28 (d, ^3J = 8.7 Hz, 4H), 5.99 (t, ^3J = 6 Hz, 2H), 4.29 (m, 4H), 3.42 (m, 4H), 2.44 (m, 4H), 2.05 (m, 8H), 1.68 (m, 4H), −2.85 ppm (s, 4H); ES^+-MS: *m/z*: 1558.8 ($[M+K]^+$), 1542.7 ($[M+Na]^+$), 1520.7 ($[M+H]^+$), 884.6 ($[M-PorphPhO(CH_2)_3+K]^+$), 868.5 ($[M-PorphPhO(CH_2)_3+Na]^+$), 846.7 ($[M-PorphPhO(CH_2)_3+H]^+$).

1:1 condensation product 9: ^1H NMR (300 MHz, $CDCl_3$), δ = 8.96 (m, 6H), 8.80 (m, 8H), 8.16 (m, 6H), 8.05 (d, ^3J = 8.7 Hz, 2H), 7.25 (d, ^3J = 8.7 Hz, 2H), 4.24 (t, ^3J = 5.7 Hz, 2H), 3.27 (t, ^3J = 6.5 Hz, 2H), 3.00 (m, no integration due to water peak), 2.38 (t, ^3J = 6.6 Hz, 2H), 1.97 (m, 4H), 1.66 (m, 4H), −2.92 ppm (s, 2H); CI-MS: 804 ($[M+H]^+$), 634 ($[M-(CH_2)_4CONH(CH_2)_4NH_2+H]^+$).

Synthesis of 10: Compound **8** (23 mg, 15 μmol) was dissolved in $CHCl_3$/MeCN/MeOH (1:3:2 mL) at 70°C. Excess MeI (1.5 mL) was added, and the heating was maintained for 8 h in the dark. After the mixture had been cooled to room temperature, the porphyrin was precipitated with Et_2O (50 mL). The red-brown precipitate was filtered on a fritted glass (porosity 4), washed with Et_2O and CH_2Cl_2, taken in the minimum amount of hot MeCN/MeOH (1:1) and dried under vacuum. Yield 98% (35 mg); purple-brown solid; ^1H NMR (300 MHz, CD_3CN), δ = 9.04 (m, 28H), 8.81 (m, 12H), 8.12 (d, ^3J = 8.7 Hz, 4H), 7.37 (d, ^3J = 8.7 Hz, 4H), 6.53 (brt, ^3J = 5.7 Hz, 2H), 4.67 (s, 12H), 4.66 (s, 6H), 4.29 (m, 4H), 3.23 (m, 4H), 2.30 (t, ^3J = 7.2 Hz, 4H), 1.53 (m, 8H), 1.26 (m, 4H), −2.93 (s, 4H); ES^+-MS: *m/z* (as PF_6 salt): 1095.1 ($[M-2PF_6]^{2+}$), 681.7 ($[M-3PF_6]^{3+}$), 475.1 ($[M-4PF_6]^{4+}$).

Synthesis of 4·NiNi: Compound **10** (35 mg, 14 μmol) and nickel(II) acetate tetrahydrate (3 equiv, 7.5 mg) were heated in DMF (3 mL) and 2,4,6-collidine (0.5 mL) at 110°C in the dark for 5 h. The product was precipitated with Et_2O (40 mL), filtered on a fritted glass (porosity 4), washed with Et_2O and CH_2Cl_2, taken in MeOH/H_2O (1:1) and dried. Anion exchange was performed on DOWEX 1×8–200 resin (chloride form) by stirring a suspension of the porphyrin in MeOH/H_2O (1:2, 15 mL) at room temperature for 4 h. The resin was filtered on a fritted glass (porosity 4) and washed with MeOH and H_2O. The solvents were evaporated and the product was dried under vacuum. Yield 92% (25 mg); red-orange solid; ES^+-MS: *m/z*: 867.50 $[M-4Cl^--4CH_3+H^+]^{2+}$, 860.50 $[M-4Cl^--5CH_3+2H^+]^{2+}$, 852.50 $[M-4Cl^--6CH_3+3H^+]^{2+}$, 578.69 $[M-4Cl^--4CH_3+H^+]^{3+}$, 573.40 $[M-4Cl^--5CH_3+2H^+]^{3+}$, 568.74 $[M-4Cl^--6CH_3+3H^+]^{3+}$; UV/Vis ($H_2O$) λ_{max} (ε) = 422 (160500), 538 nm (15200 $mol^{-1}Lcm^{-1}$).

Synthesis of 4·MnMn: Compound **10** (16 mg, 6.5 μmol) and manganese(II) acetate tetrahydrate (8 equiv, 12.5 mg) were heated in DMF (1 mL) and 2,4,6-collidine (0.5 mL) at 110°C in the dark for 3 h. A second batch of $Mn(OAc)_2{\cdot}4H_2O$ (8 equiv, 12.5 mg) was added as an aqueous solution (0.5 mL), and heating was maintained for an additional 3 h. The product was precipitated as a hexafluorophosphate salt by adding saturated aqueous KPF_6, filtered on a fritted glass (porosity 3), washed with water, taken in acetone and dried. Anion exchange was performed on DOWEX 1×8–200 resin (chloride form) by stirring the porphyrin in water (10 mL) at 50°C for 90 h. The resin was filtered on a fritted glass (porosity 3) and washed with MeOH, MeCN and water. The solvents were evaporated, the product was taken in MeOH and precipitated with diethyl ether. The precipitate was filtered, washed with Et_2O, taken in MeOH and dried. Yield 96% (12.5 mg); green-brown solid; ES^+-MS: *m/z*: 357.7 $[M-6Cl^-]^{5+}$; UV/Vis (H_2O) λ_{max} (ε) = 466 (120000 $mol^{-1}Lcm^{-1}$).

Surface plasmon resonance (BIACORE) analysis

Principle: Binding events between two molecules were monitored in real time, without the use of any label, by using an optical phenomenon called surface plasmon resonance (SPR). Biomolecular binding events cause changes in the refractive index close to the surface layer of a chip that are detected as changes in the SPR signal. During a binding analysis, SPR changes occur as a solution is passed over the surface of a sensor chip. To perform an analysis, one interactant (ligand) is immobilized over a carboxymethylated dextran matrix of a sensor chip. The sensor surface forms one wall of a flow cell. A sample containing the other interactant (analyte) is injected over this surface in a precisely controlled flow. The progress of interaction is monitored as a sensorgram that expresses resonance units (RU) as a function of time. The analyte binds to the surface-attached ligand during sample injection; this results in an increase in signal. At the end of the injection, the sample is replaced by a continuous flow of buffer, and the decrease in signal reflects dissociation of interactant from the surface-bound complex.

Materials: All binding studies based on the SPR phenomenon were performed on a four-channel BIACORE 3000 optical biosensor instrument (BIAcore AB, Uppsala, Sweden). All experiments were performed on sensor chips SA (sensor chips with streptavidin covalently immobilized on a carboxymethylated dextran matrix) obtained from BIAcore AB, Uppsala, Sweden.

Immobilization of biotinylated DNA probes: Both flow cells of an SA streptavidin sensor chip were coated with biotinylated probes. Three 5′-biotin-labelled oligonucleotide sequences (Eurogentec, Belgium) were used in these experiments. Two hairpin duplexes were chosen from previous published work,[36] referred to as the 22-mer $[(CG)_4]$, (5′-TTCGCGCGCGTTTTCGCGCGCG sequence; 303 RU immobilized on flow cell 2) and the 20-mer [AATT] (5′-CGAATTCGTCTCCGAATTCG sequence; 333 RU immobilized on flow

cell 3) and the human telomeric quadruplex DNA, referred to as the 22-mer [G_4], corresponding to 5′-AGGGTTAGGGTTAGGGTTAGGG sequence (328 RU immobilized on flow cell 4). No target oligonucleotide was captured on flow cell 1, so it could be used as a reference surface. All immobilization steps were performed at a final DNA concentration of 10 nM and at a flow rate of 2 $\mu L\,min^{-1}$. Injections were stopped when sufficient RU levels were obtained.

BIA analysis: Binding analyses were performed with multiple injections of different compound concentrations over the immobilized DNA surface at 25 °C. All samples were diluted in HBS-EP/KCl buffer and were injected over the sensor surface for 5 min at a flow rate of 20 $\mu L\,min^{-1}$. All diluted samples were injected at the same time over the four channels (flow cells). Flow cell 1 was used to obtain control sensorgrams showing nonspecific binding to the streptavidin-coated surface as well as refractive-index changes resulting from changes in the bulk properties of each solution. Control sensorgrams were subtracted from sensorgrams obtained with immobilized DNAs to yield true binding responses. Kinetics constants were calculated by using BIAevaluation 4.0.1 software and apparent association constants (K_a) were calculated as the ratio of k_{on}/k_{off}.

For each molecule, we calculated k_{on}, k_{off} and K_a constants using both one-site (Langmuir) and two-site algorithms and selected the better fit corresponding to the lower Chi2 parameter value (not shown).

Scatchard analysis: For all the molecules tested, data obtained from sensorgrams were used for Scatchard analysis by using the equation:

$$R_{eq}/C = K_a\,(R_{max} - R_{eq})$$

here R_{eq} is the response at equilibrium in resonance units (RU), C is the concentration of analyte in solution [nM] and R_{max} is the theoretical maximum response (proportional to the amount of immobilized ligand). R_{eq} was calculated by BIAevaluation 4.0.1 software. As R_{max} remains constant, a plot of R_{eq}/C versus R_{eq} has a slope of $-K_a$ in the case of the one-site model of interaction. The one-site or nonequivalent two-site model of interaction was determined from Scatchard plots.

Telomeric repeat amplification protocol, TRAP assay: Exponentially growing HeLa cell cultures were trypsinized, washed in PBS and S-100 extracts obtained as described.[40] Stock-protein concentration was adjusted to 5 $\mu g\,mm^{-3}$, flash-frozen and stored at −80 °C. To assess telomerase activity, compounds were serially diluted in lysis buffer (range, 50 μM to 25 nM) and mixed 1:1 with HeLa cell extract (1.25 μg; final volume 5 mm^3). Extension and amplification reactions and electrophoresis were carried out as described.[40] For quantification, autoradiographs were scanned in a Storm 860 scanner, and the signal intensity of telomerase ladder and PCR internal control (ITAS) were measured by using ImageQuant v1.2 software. Dose-dependent PCR inhibition was observed (diminished or absent internal control (ITAS) signal at concentrations >25 μM); these data points were therefore excluded from analysis. Regression curves and IC_{50} values were calculated by using GraphPad Prism software, and values were expressed as percentage activity of an equal amount of untreated HeLa cell extract. Negative controls were included in all assays by preincubating HeLa extracts with RNAse for 10 min at 30 °C prior to the extension reaction. All compounds were assayed in at least two separate TRAP assays; regression curves for each compound were highly reproducible.

Acknowledgements

We thank the CNRS for financial support. I.M.D. thanks the "Ligue Nationale contre le Cancer" for a postdoctoral fellowship. The SPR work was supported in part by grants from the "ARECA protein and cancer" network from the "Association pour la Recherche sur le Cancer" (ARC). Research in the laboratory of M.A.B. is funded by the MCYT (SAF2001-1869, GEN2001-4856-C13-08), by the Regional Government of Madrid, CAM (08.1/0054/01), by the European Union (TELOSENS FIGH-CT.2002-00217, INTACT LSHC-CT-2003-506803, ZINCAGE FOOD-CT-2003-506850, RISC-RAD F16R-CT-2003-508842), and the Josef Steiner Cancer Award 2003. A.M.T. is a postdoctoral fellow of Fundación Carolina.

Keywords: antitumor agents · G-quadruplex DNA · porphyrins · surface plasmon resonance · TRAP assay

[1] E. H. Blackburn, *Nature* **1991**, *350*, 569 – 573.
[2] R. J. Wellinger, D. Sen, *Eur. J. Cancer* **1997**, *33*, 735 – 749.
[3] T. Simonsson, P. Pecinka, M. Kubista, *Nucleic Acids Res.* **1998**, *26*, 1167 – 1172.
[4] A. Siddiqui-Jain, C. L. Grand, D. J. Bearss, L. H. Hurley, *Proc. Natl. Acad. Sci. USA* **2002**, *99*, 11 593 – 11 598.
[5] P. Weisman-Shomer, M. Fry, *J. Biol. Chem.* **1993**, *268*, 3306 – 3312.
[6] S. Lyonnais, C. Hounsou, M.-P. Teulade-Fichou, J. Jeusset, E. Le Cam, G. Mirambeau, *Nucleic Acids Res.* **2002**, *30*, 5276 – 5283.
[7] S. Lyonnais, R. J. Gorelick, J.-L. Mergny, E. Le Cam, G. Mirambeau, *Nucleic Acids Res.* **2003**, *31*, 5754 – 5763.
[8] G. Fang, T. R. Cech, *Cell* **1993**, *74*, 875 – 885.
[9] N. Baran, L. Pucshansky, Y. Marco, S. Benjamin, H. Manor, *Nucleic Acids Res.* **1997**, *25*, 297 – 303.
[10] H. Sun, J.K. Karow, I. D. Hickson, N. Maizels, *J. Biol. Chem.* **1998**, *273*, 27 587 – 27 592.
[11] M. Fry, L. Loeb, *J. Biol. Chem.* **1999**, *274*, 12 797 – 12 802.
[12] H. Sun, A. Yabuki, N. Maizels, *Proc. Natl. Acad. Sci. USA* **2001**, *98*, 12 444 – 12 449.
[13] H. Fukuda, M. Katahira, Y. Tsuchiya, Y. Enokizono, T. Sugimura, M. Nagao, H. Nakagama, *Proc. Natl. Acad. Sci. USA* **2002**, *99*, 12 685 – 12 690.
[14] H. Han, L. H. Hurley, *Trends Pharmacol. Sci.* **2000**, *21*, 136 – 142.
[15] J.-L. Mergny, J.-F. Riou, P. Mailliet, M.-P. Teulade-Fichou, E. Gilson, *Nucleic Acids Res.* **2002**, *30*, 839 – 865.
[16] Y. Wang, D. J. Patel, *Structure* **1993**, *1*, 263 – 282.
[17] G. N. Parkinson, M. P. H. Lee, S. Neidle, *Nature* **2002**, *417*, 876 – 880.
[18] A. T. Phan, D. J. Patel, *J. Am. Chem. Soc.* **2003**, *125*, 15 021 – 15 027.
[19] R. T. Wheelhouse, D. Sun, H. Han, F. X. Han, L. H. Hurley, *J. Am. Chem. Soc.* **1998**, *120*, 3261 – 3262.
[20] O. Y. Fedoroff, M. Salazar, H. Han, V. V. Chemeris, S. M. Kerwin, L. H. Hurley, *Biochemistry* **1998**, *37*, 12 367 – 12 373.
[21] a) M. Read, R. J. Harrison, B. Romagnoli, F. A. Tanious, S. H. Gowan, A. P. Reszka, W. D. Wilson, L. R. Kelland, S. Neidle, *Proc. Natl. Acad. Sci. USA* **2001**, *98*, 4844 – 4849; b) R. J. Harrison, J. Cuesta, G. Chessari, M. A. Read, S. K. Basra, A. P. Reszka, J. Morrell, S. M. Gowan, C. M. Incles, F. A. Tanious, W. D. Wilson, L. R. Kelland, S. Neidle, *J. Med. Chem.* **2003**, *46*, 4463 – 4476.
[22] S. M. Gowan, R. Heald, M. F. G. Stevens, L. R. Kelland, *Mol. Pharmacol.* **2001**, *60*, 981 – 988.
[23] J.-L. Mergny, L. Lacroix, M.-P. Teulade-Fichou, C. Hounsou, L. Guittat, M. Hoarau, P. B. Arimondo, J.-P. Vigneron, J.-M. Lehn, J.-F. Riou, T. Garestier, C. Hélène, *Proc. Natl. Acad. Sci. USA* **2001**, *98*, 3062 – 3067.
[24] K. Shin-ya, K. Wierzba, K. Matsuo, T. Ohtani, Y. Yamada, K. Furihata, Y. Hayakawa, H. Seto, *J. Am. Chem. Soc.* **2001**, *123*, 1262 – 1263.
[25] M. Y. Kim, H. Vankayalapati, K. Shin-ya, K. Wierzba, L. H. Hurley, *J. Am. Chem. Soc.* **2002**, *124*, 2098 – 2099.
[26] J.-F. Riou, L. Guittat, P. Mailliet, A. Laoui, E. Renou, O. Petitgenet, F. Mégnin-Chanet, C. Hélène, J.-L. Mergny, *Proc. Natl. Acad. Sci. USA* **2002**, *99*, 2672 – 2677.

[27] M.-P. Teulade-Fichou, C. Carrasco, L. Guittat, C. Bailly, P. Alberti, J.-L. Mergny, A. David, J.-M. Lehn, W. D. Wilson, *J. Am. Chem. Soc.* **2003**, *125*, 4732 – 4740.
[28] G. R. Clark, P. D. Pytel, C. J. Squire, S. Neidle, *J. Am. Chem. Soc.* **2003**, *125*, 4066 – 4067.
[29] Q. Chen, I. D. Kuntz, R. H. Shafer, *Proc. Natl. Acad. Sci. USA* **1996**, *93*, 2635 – 2639.
[30] J. A. Schouten, S. Ladame, S. J. Mason, M. A. Cooper, S. Balasubramanian, *J. Am. Chem. Soc.* **2003**, *125*, 5594 – 5595.
[31] S. Prince, F. Körber, P. R. Cooke, J. R. Lindsay Smith, M. A. Mazid, *Acta Crystallogr.* **1993**, *C49*, 1158 – 1160.
[32] C. Vialas, G. Pratviel, B. Meunier, *Biochemistry* **2000**, *39*, 9514 – 9522.
[33] A. Maraval, S. Franco, C. Vialas, G. Pratviel, M. A. Blasco, B. Meunier, *Org. Biomol. Chem.* **2003**, *1*, 921 – 927.
[34] L. Ding, C. Casas, G. Etemad-Moghadam, B. Meunier, *New J. Chem.* **1990**, *14*, 421 – 431.
[35] P. Bigey, S. Frau, C. Loup, C. Claparols, J. Bernadou, B. Meunier, *Bull. Soc. Chim. Fr.* **1996**, *133*, 679 – 689.
[36] C. Carrasco, F. Rosu, V. Gabelica, C. Houssier, E. De Pauw, C. Garbay-Jaureguiberry, B. Roques, W. D. Wilson, J. B. Chaires, M. J. Waring, C. Bailly, *ChemBioChem* **2002**, *3*, 1235 – 1241.
[37] J. A. Strickland, L. G. Marzilli, K. M. Gay, W. D. Wilson, *Biochemistry* **1988**, *27*, 8870 – 8878.
[38] M. A. Sari, J. P. Battioni, D. Dupré, D. Mansuy, J. B. Le Pecq, *Biochemistry* **1990**, *29*, 4205 – 4215.
[39] L. Ding, J. Bernadou, B. Meunier, *Bioconjugate Chem.* **1991**, *2*, 201 – 206.
[40] M. A. Blasco, M. Rizen, C. W. Greider, D. Hanahan, *Nat. Genet.* **1996**, *12*, 200 – 204.

Received: April 21, 2004
Early View Article
Published online on November 18, 2004

